THE JOURNAL OF BIOLOGICAL CHEMISTRY VOL. 291, NO. 9, pp. 4323–4333, February 26, 2016

Rapid Remodeling of Invadosomes by G_i-coupled Receptors

DISSECTING THE ROLE OF Rho GTPases[*][S]

Received for publication, October 9, 2015, and in revised form, January 5, 2016 Published, JBC Papers in Press, January 6, 2016, DOI 10.1074/jbc.M115.695940

Katarzyna M. Kedziora[‡], Daniela Leyton-Puig[‡], Elisabetta Argenzio[‡], Anja J. Boumeester[‡], Bram van Butselaar[‡], Taofei Yin[§], Yi I. Wu[§], Frank N. van Leeuwen[¶], Metello Innocenti[‖], Kees Jalink[‡1,2], and Wouter H. Moolenaar[‡1]

From the [‡]Division of Cell Biology and [‖]Division of Molecular Genetics, Netherlands Cancer Institute, Amsterdam 1066 CX, The Netherlands, the [§]Center for Cell Analysis and Modeling, University of Connecticut Health Center, Farmington, Connecticut 06030, and the [¶]Department of Cell Biology, Radboud University Medical Centre, 6525 GA Nijmegen, The Netherlands

Invadosomes are actin-rich membrane protrusions that degrade the extracellular matrix to drive tumor cell invasion. Key players in invadosome formation are c-Src and Rho family GTPases. Invadosomes can reassemble into circular rosette-like superstructures, but the underlying signaling mechanisms remain obscure. Here we show that Src-induced invadosomes in human melanoma cells (A375M and MDA-MB-435) undergo rapid remodeling into dynamic extracellular matrix-degrading rosettes by distinct G protein-coupled receptor agonists, notably lysophosphatidic acid (LPA; acting through the LPA_1 receptor) and endothelin. Agonist-induced rosette formation is blocked by pertussis toxin, dependent on PI3K activity and accompanied by localized production of phosphatidylinositol 3,4,5-trisphosphate, whereas MAPK and Ca^{2+} signaling are dispensable. Using FRET-based biosensors, we show that LPA and endothelin transiently activate Cdc42 through G_i, concurrent with a biphasic decrease in Rac activity and differential effects on RhoA. Cdc42 activity is essential for rosette formation, whereas $G_{12/13}$-mediated RhoA-ROCK signaling suppresses the remodeling process. Our results reveal a G_i-mediated Cdc42 signaling axis by which G protein-coupled receptors trigger invadosome remodeling, the degree of which is dictated by the Cdc42-RhoA activity balance.

Invadopodia are cancer-specific, actin-rich membrane protrusions that are associated with proteolytic degradation of the extracellular matrix (ECM),[3] thereby driving tumor cell invasion into surrounding tissues (1–5). Similar protrusive structures, termed podosomes, are found in various non-malignant cells, notably osteoclasts, macrophages, and endothelial cells (1, 5); however, invadopodia degrade the ECM more aggressively than do podosomes (6). Recent studies have shown important roles for functional invadopodia/podosomes *in vivo*, during tumor cell extravasation, metastasis, and angiogenesis as well as during morphogenetic movements *in vivo* (7–10).

Invadopodia and podosomes, collectively called invadosomes, consist of a core of F-actin and various actin-associated structural and regulatory proteins (1, 2, 4, 5). One major player in the formation and maintenance of invadosomes is the Src tyrosine kinase, which phosphorylates invadopodial substrates, such as cortactin and the scaffold protein Tks5 (tyrosine kinase substrate 5) (2, 11). Therefore, cells expressing active Src are a convenient system for studying the regulation of invadosomes. Additional key players in invadosome formation are the actin-regulatory Rho GTPases, in particular Cdc42, Rac, and RhoA (12, 13). Active Cdc42 stimulates the formation of invadosomes (12), whereas Rac activity is thought to promote their disassembly (14). Other signaling molecules implicated in invadosome formation are phosphoinositide 3-kinase (PI3K), ERK1/2/MAPK, and cytosolic free calcium (6, 15). The maturation of invadosome precursors into ECM-degrading structures is a dynamic process that is regulated by growth factors such as epidermal growth factor (EGF), platelet-derived growth factor (PDGF), vascular endothelial growth factor (VEGF), and transforming growth factor-β (TGF-β) (4, 16–18).

Interestingly, individual invadosomes can assemble into higher-order "rosettes" consisting of giant circular arrays of F-actin. Rosettes are observed in some cancer cells (19, 20), v-Src-transformed fibroblasts (21), osteoclasts (22), and endothelial cells (9, 23). Invadosome rosettes may remodel the ECM more efficiently and in a more localized manner than do individual invadosomes (20). Evidence for invadosome rosettes in human tissues is emerging, for example, in the vasculature of lung tumors (9). However, the signal inputs and pathways that drive the remodeling of pre-existing invadosomes into rosettes remain largely unknown.

Here we examine how distinct GPCR agonists, notably lysophosphatidic acid (LPA) and endothelin, influence the behavior of Src-induced invadosomes in human A375M melanoma cells. LPA is a multifunctional lipid mediator and a major serum constituent that signals through six distinct GPCRs (LPA_{1-6}) (24, 25). LPA is produced by autotaxin, a secreted lysophospholipase D originally identified as a motility factor for melanoma cells (26, 27). Autotaxin-LPA

* This work was funded by Dutch Cancer Society Grant NKI2010-4626, Stichting Technische Wetenschappen Grant 12150, and Nederlandse Organisatie voor Wetenschappelijk Onderzoek Grant 91106027 (to K. J.) and National Institutes of Health Grant NS071216 (to Y. I. W.). The authors declare that they have no conflict of interest with the contents of this article. The content is solely the responsibility of the authors and does not necessarily represent the official views of the National Institutes of Health.

[S] This article contains supplemental Videos 1 and 2.

[1] Co-senior authors.

[2] To whom correspondence should be addressed: Division of Cell Biology, Netherlands Cancer Institute, Plesmanlaan 121, 1066 CX Amsterdam, The Netherlands. Tel.: 31-20-512-1933; E-mail: k.jalink@nki.nl.

[3] The abbreviations used are: ECM, extracellular matrix; GPCR, G protein-coupled receptor; LPA, lysophosphatidic acid; PIP_3, phosphatidylinositol 3,4,5-trisphosphate; PTX, pertussis toxin; S1P, sphingosine 1-phosphate; PH, pleckstrin homology; GEF, GDP/GTP exchange factor; CFP, cyan fluorescent protein; BAPTA-AM, 1,2-bis(*o*-aminophenoxy)ethane-*N*,*N*,*N*′,*N*′-tetraacetic acid tetra(acetoxymethyl)ester.

signaling promotes invasive cell migration and experimental metastasis (28–30), but little is known about how LPA may affect invadosome behavior. Endothelin is produced by stromal and tumor cells and signals in an autocrine or paracrine manner to promote malignant cell behavior; acting through the endothelin B receptor, endothelin is strongly implicated in melanoma progression (31–33).

We show here that LPA and endothelin induce the rapid transition of the ECM-degrading invadosome cluster into highly dynamic rosettes through G_i, and we analyze the underlying signaling events with a focus on Rho family GTPases. By using FRET-based biosensors, we monitor and dissect the agonist-regulated activities of RhoA, Rac1, and Cdc42 and find a key role for G_i-mediated Cdc42 activation with a likely modulatory role for Rac1 and an opposing role for RhoA. Our results provide new insights into how certain GPCRs remodel invadosomes, thereby rapidly redistributing ECM-degrading activity.

Experimental Procedures

Reagents—LPA (1-oleyl) and S1P were from Avanti Polar Lipids. Endothelin and thrombin receptor-activating peptide were from Sigma. Fura Red-AM, Oregon Green 488, phalloidin-Alexa488, and phalloidin-Alexa568 were from Invitrogen. SuperScript RT and OG gelatin were from Invitrogen. The GeneJet RNA purification kit was from Thermo Scientific. Pertussis toxin was from Gibco. FastStart Universal SYBR Green Master (Rox) was from Roche Applied Science. Ki16425 was from Santa Cruz Biotechnology, Inc., and PLX4720 was from Selleckchem. Antibodies used were as follows: polyclonal rabbit anti-p44/42 and monoclonal anti-phospho-p44/42 MAPK (Cell Signaling), anti-actin (Sigma), anti-Cdc42 (Santa Cruz Biotechnology), and anti-Akt and anti-phospho-Akt (Cell Signaling). Secondary antibodies were conjugated to HRP (Dako). Plasmids used were as follows: GRP1-GFP (45) and Tks5-eGFP (a gift from Dr. Sara Courtneidge).

Cells and Transfections—A375M, MDA-MB-435, and HEK293 cells were cultured in DMEM (10% FCS), and antibiotics (penicillin and streptomycin) were cultured under 5% CO_2 at 37 °C. Cells were transfected using Lipofectamine2000. Src(Y530F) (chicken), LifeAct-mCherry, and GFP-actin were stably introduced into A375M cells by retroviral transduction. c-Src(Y530F) was introduced into LZRS-Neo vector with BamHI/NotI. GFP-actin and LifeAct-mCherry were used in the LZRS-Zeo vector. Viral particles were created in AmphoPack293 cells. Cells were selected with 1 mg/ml G418 (LZRS-SrcYF) or 1 mg/ml Zeocin (LZRS-GFP-actin). Empty vectors (LZRS-Neo and LZRS-Zeo) were used as controls. In MDA-MB-435 cells, active c-Src(YF) was introduced by transient transfection.

Immunofluorescence Analysis—Primary antibodies used were as follows: cortactin (1:200; Millipore), FAK (1:200; Transduction Laboratories), vinculin (1:400; Abcam, Cambridge, UK), and pY20 (1:200; BD Biosciences, Erembodegem, Belgium). Secondary antibodies used were as follows: goat anti-mouse Alexa488 IgG (1:200; Molecular Probes) and goat anti-mouse Alexa532 IgG (1:200; Molecular Probes). Cells were seeded on glass uncoated coverslips (24 mm) for 48 h, serum-starved for >2 h, stimulated, washed with PBS, fixed with 4% paraformaldehyde in PBS (10 min), permeabilized with 0.1% Triton X-100 in PBS (2 min), blocked in 3% BSA (PBS, room temperature, 1 h), and stained with selected antibodies (in 3% BSA in PBS). F-actin was detected using phalloidin-Alexa488 or phalloidin-Alexa568 (1 unit/ml).

Knockdown Experiments—LPAR1 shRNAs were as follows: shRNA 1, GCCATCGTTATGGGTGCTATA; shRNA 2, CCTATTGGTCATGGTGGCAAT; shRNA 3, GCCTATGAGAAATTCTTCCTT; shRNA 4, CGGGATACCATGATGAGTCTT. Cdc42 shRNAs were as follows: shRNA 1, CGGAATATGTACCGACTGTTT; shRNA 2, CCTGATATCCTACACAACAAA; shRNA 3, CAGATGTATTTCTAGTCTGTT; shRNA 4, CCCTCTACTATTGAGAAACTT.

Hairpins were introduced using the pLKO lentiviral vector (empty pLKO vector as a negative control). Viral particles were produced in HEK293 cells transfected with calcium phosphate. Transduced cells were imaged or harvested for total mRNA extraction after 48 h.

Matrix Degradation Assay—Coverslips were coated with gelatin as described previously (59). To determine degradative capacity, 100,000 cells/coverslip were seeded in serum-free DMEM (with or without GM6001). After 48 h, coverslips were washed with PBS and fixed with 4% paraformaldehyde, and cells were stained with phalloidin. Gelatin degradation was determined from confocal images of >20 fields of view/coverslip, using 2 coverslips/condition in two independent experiments (4 coverslips/condition). For time lapse imaging, cells expressing GFP-actin were plated on coverslips coated with gelatin-ATTO-633 for 24 h.

Live Cell Imaging—Cells were seeded on glass coverslips (24 mm) for 24–72 h in DMEM (10% FCS) and serum-starved >2 h before experiments. Cells were imaged in DMEM/F-12 at 37 °C in a humidified chamber at 5% CO_2 using a TCS SP5 confocal microscope (Leica Microsystems) with a ×63, 1.4 numerical aperture oil immersion objective. The pinhole was set to 1.5 Airy units, and focus was set to the ventral membrane of the cells. We took great care to excite at minimal laser intensity to avoid photobleaching or phototoxicity.

Wide Field FRET Experiments—Experiments were performed in HEPES-buffered saline (containing 140 mM NaCl, 5 mM KCl, 1 mM $MgCl_2$, 1 mM $CaCl_2$, 10 mM glucose, 10 mM HEPES), pH 7.2, at 37 °C. Cells were plated on uncoated coverslips and transfected 24 h before experiments with the indicated biosensors were placed on a thermostatted (37 °C) inverted Nikon Diaphot microscope and excited at 425 nm. Donor and acceptor emission were detected simultaneously with two photomultipliers, using a 505-nm beam splitter and optical filters: 470 ± 20 nm (CFP channel) and 530 ± 25 nm (YFP channel). FRET was expressed as the ratio between acceptor and donor signals, set at 1 at the onset of the experiment.

Rho GTPase Biosensors—The design of FRET-based biosensors of Rac1, Cdc42, and RhoA was based on the design of the Raichu sensors (34, 35) and FLARE-RhoA (36) (details to be described elsewhere). Briefly, the complete amino acid sequence of a given Rho GTPase was positioned at the C terminus of a single polypeptide chain to preserve its interaction with GDI and other regulatory proteins. A FRET pair consisting of Cerulean3 and circularly permutated Venus was used. The CRIB domain of PAK and HR1 region of PKN were used as the

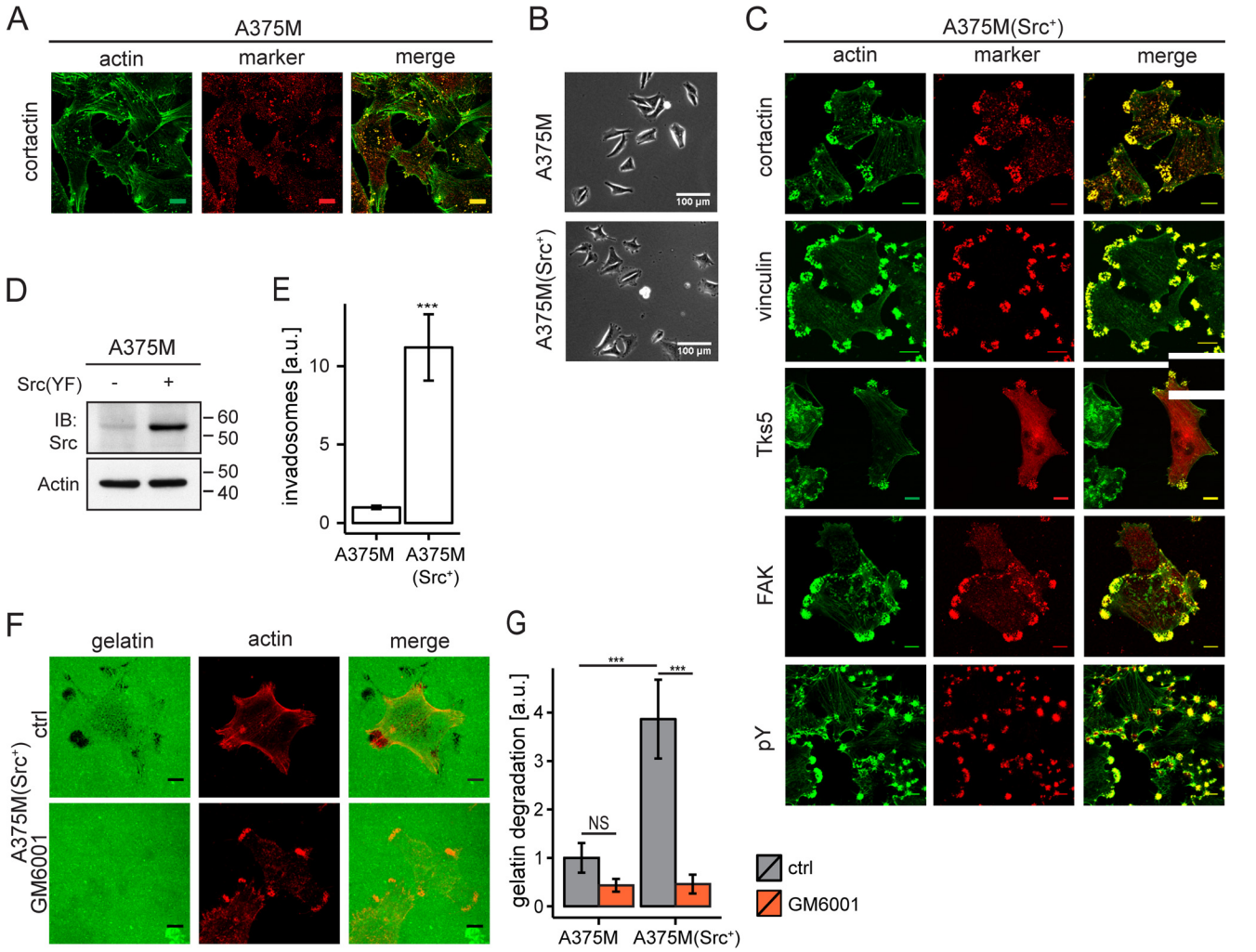

FIGURE 1. **Functional invadosomes in A375M melanoma cells and effects of activated c-Src.** *A*, human A375M melanoma cells produce punctate invadosome structures. Confocal images show colocalization of F-actin and cortactin. *Scale bar*, 10 μm. *B*, phase-contrast images of A375M and Src(YF)-expressing A375M(Src$^+$) cells. *Scale bar*, 100 μm. *C*, Src-induced invadosome clusters in A375M(Src$^+$) cells. Confocal images show colocalization of actin and the indicated invadosomal markers (cortactin, vinculin, Tks5-GFP, and focal adhesion kinase (*FAK*)) and phosphotyrosine (*pY*) at the ventral plasma membrane. *Scale bar*, 10 μm. *D*, Western blotting showing c-Src expression in A375M and A375M(Src+) cells. Actin was used as a loading control. *E*, invadosomes in A375M and A375M(Src$^+$) cells quantified as a fraction of the ventral membrane area containing actin and cortactin (about 100 fields from four separate coverslips). *Error bars*, S.E.; two-tailed *p* values were determined by Wilcoxon signed-rank test; ***, $p < 0.001$. *F*, localized gelatin degradation by A375M(Src$^+$) cells at the invadosome clusters. Representative confocal images show fluorescent gelatin with and without metalloprotease inhibitor GM6001 (10 μM). *Dark spots* are indicative of gelatin degradation. *Scale bar*, 10 μm. *G*, quantification of gelatin degradation in A375M *versus* A375M(Src$^+$) cells; GM6001 concentration, 10 μM. Two-tailed *p* values were determined by Wilcoxon signed rank test; ***, $p < 0.001$. Quantification was done of ~100 fields from two separate coverslips. *a.u.*, arbitrary units.

effector domain for activated Rac1/Cdc42 and RhoA, respectively. In control biosensors, point mutations (H83D/H86D in PAK and L59Q in PKN) were introduced to generate binding-deficient effector domains, so that FRET ratios remained at the basal level regardless of the activation state of the Rho GTPases.

Confocal FRET Experiments—Cells transfected with a given biosensor were imaged on the TCS SP5 confocal microscope using a Leica ×63, 1.4 numerical aperture "lambda-blue" oil immersion objective. Excitation was at 442 nm, and the FRET ratio was determined from emission images acquired simultaneously at 448–505 nm (CFP channel) and at 505–555 nm (YFP channel) and expressed as a ratio (YFP/CFP). In these cells, LifeAct-mCherry was imaged simultaneously in the range 568–650 nm.

Ca^{2+} Imaging—Intracellular [Ca^{2+}] was detected essentially as published (60). Experiments were done in serum-free DMEM/F-12, using a Leica SP5 confocal microscope with excitation at 488 nm and emission at two channels (495–550 nm and 560–650 nm). The confocal pinhole was fully opened, and recordings were normalized by setting basal levels to 1.0.

Image Analysis—Invadosomes were detected by intensity and size segmentation of colocalizing actin and cortactin signals after manual thresholding using Fiji software (37) and normalized to control cells. At least three independent experiments were analyzed for every condition (18 fields of view/condition, 5–10 cells/field of view, >100 cells/condition).

Western Blotting—Cells were plated in 6-well plates, serum-starved overnight, treated with inhibitors (U0126 (10 μM) for 1 h, PLX4720 (1 μM) for 2 h, wortmannin (100 nM) for 15 min, PTX (200 ng/ml) overnight) and stimulated with agonists as indicated. Whole-cell lysates were prepared by scraping PBS-washed cells in denaturing conditions in

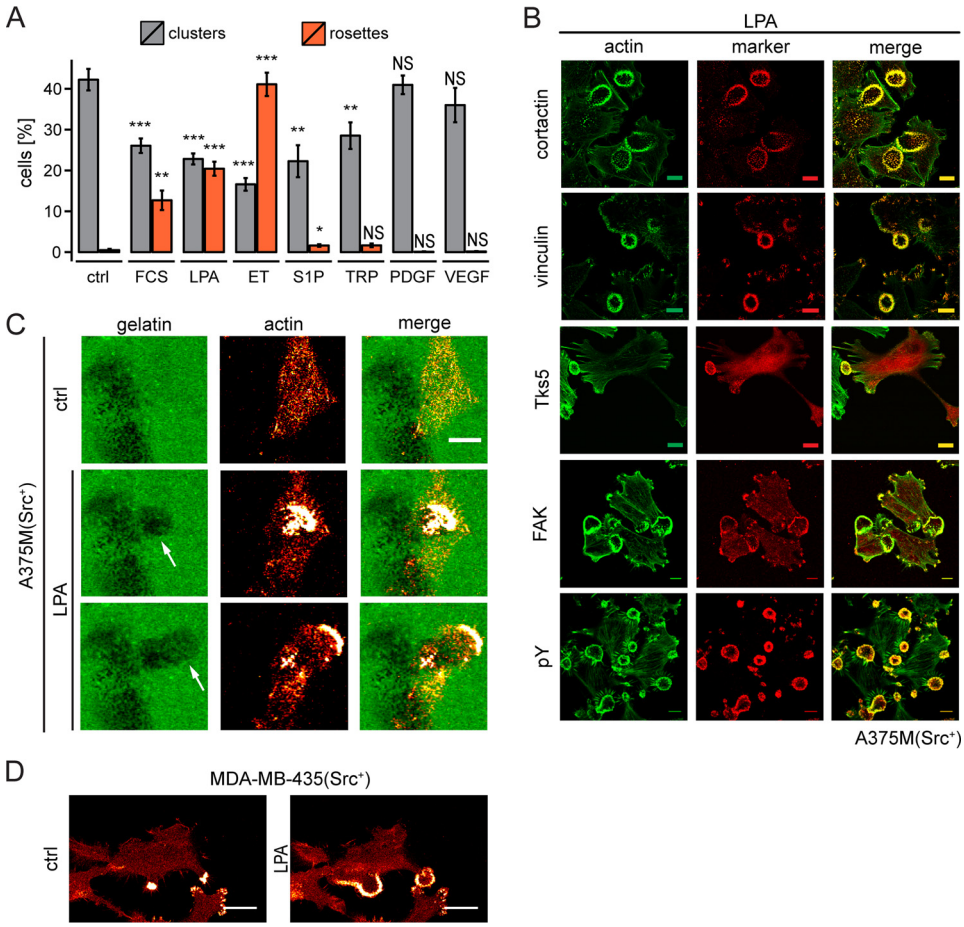

FIGURE 2. **Agonist-induced remodeling of invadosome clusters into rosettes.** *A*, A375M(Src$^+$) cells stimulated with the indicated agonists and examined for rosette formation from invadosome clusters. The graph shows the percentage of cells showing clusters *versus* rosettes at 2.5 min after stimulation by agonist addition. LPA, endothelin (*ET*), and S1P were used for further studies. *TRP*, thrombin receptor-activating peptide. *Error bars*, S.E. ($n > 6$ coverslips, at least 150 cells scored per single experiment). A two-sided Student's *t* test was used to indicate significant differences from control (*ctrl*) (unstimulated) cells; *NS*, non-significant; *, $p < 0.05$; **, $p < 0.01$; ***, $p < 0.001$. See also supplemental Video 1. *B*, rosette formation in A375M(Src$^+$) cells by LPA (5 μM; 2.5 min). Invadosomal markers were as indicated. *Scale bar*, 10 μm. *C*, LPA-induced degradation of fluorescent gelatin by a dynamic invadosome rosette in a single cell. *Dark spots* indicate sites of gelatin degradation. Confocal images were taken from a time lapse experiment (see supplemental Video 2). A single invadosome rosette degrades gelatin as it advances. *Scale bar*, 20 μm. *D*, rosette formation in human MDA-MB-435(Src$^+$) melanoma cells by LPA (5 μM; 2.5 min). *Scale bar*, 20 μm.

radioimmune precipitation assay buffer (50 mM Tris-HCl, 150 mM NaCl, 1 mM EDTA, 1% Triton X-100, 1% sodium deoxycholate, 0.1% SDS), supplemented with a protease inhibitor mixture (or, for detection of phospho-Akt, in JS lysis buffer (50 mM HEPES, pH 7.5, 150 mM NaCl, 1.5 mM $MgCl_2$, 5 mM EGTA, 1% glycerol, 1% Triton X-100) supplemented with NaO_3V_4 (5 μM), NaF (1 μM), and protease inhibitor mixture). Membranes were blocked in 3% BSA and incubated with primary antibodies (1:1000), followed by HRP-conjugated secondary antibodies (1:10,000).

LPA Receptor Expression Analysis—LPAR1–6 expression levels were determined by RT-qPCR reactions on cDNA derived from cell lysates (total mRNA isolation was followed by SuperScript cDNA synthesis), using power SYBR Green with specific primers: LPAR1, AATCGGGATACCATGATGAGT (forward) and CCAGGAGTCCAGCAGATGATAAA (reverse); LPAR2, CGCTCAGCCTGGTCAAAGACT (forward) and TTGCAGGACTCACAGCCTAAAC (reverse); LPAR3, AGGACACCCATGAAGCTAATGAA (forward) and GCCGTCGAGGAGCAGAAC (reverse); LPAR4, CCTAGTCCTCAGTGGCGGTATT (forward) and CCTTCAAAGCAGGTGGTGGTT (reverse); LPAR5, CCAGCGACCTGCTCTTCAC (forward) and CCAGTGGTGCAGTGCGTAGT (reverse); LPAR6, AAACTGGTCTGTCAGGAGAAGT (forward) and CAGGCAGCAGATTCATTGTCA (reverse). Expression levels were normalized to the expression of cyclophilin A (CATCTGCACTGCCAAGACTGA (forward) and TTGCCAAACACCACATGCTT (reverse)) and calculated according to the cycling threshold method.

Results

c-Src Induces Functional Invadosomes in Melanoma Cells—Given the key role of c-Src in invadopodia formation, we examined various human tumor cells for their ability to produce invadopodia upon expression of active c-Src and for their responsiveness to selected GPCR agonists. On the basis of these criteria, we selected metastatic A375M melanoma cells as our main model system. A375M cells showed characteristic actin-rich invadopodia that colocalized with cortactin at the ventral plasma membrane (Fig. 1*A*). Expression of constitutively active

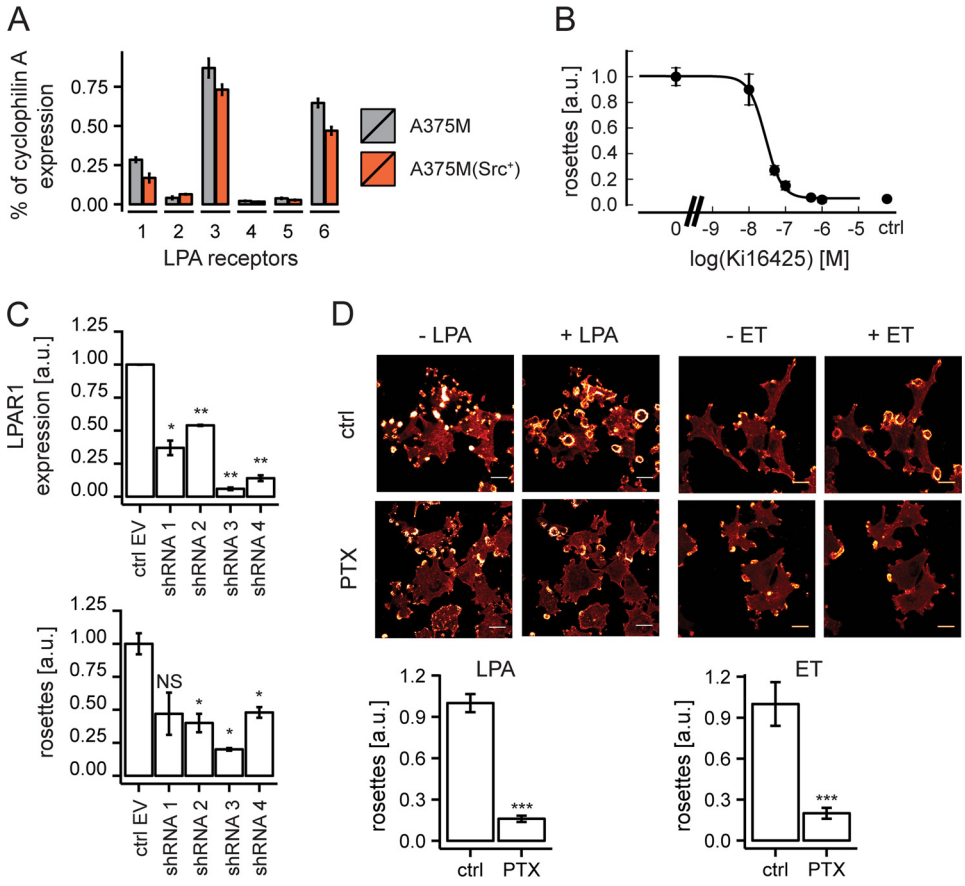

FIGURE 3. **Rosette formation mediated by the LPA_1 receptor and inhibition by PTX.** *A*, LPA receptor mRNA expression pattern in A375M and A375M(Src^+) cells as determined by qPCR. *Error bars*, S.E. ($n = 3$). *B*, dose-dependent inhibition of LPA-induced rosette formation by LPA_1 antagonist Ki16425. IC_{50} ~30 nM. *Error bars*, S.E. ($n = 3$). *C*, LPA_1 depletion inhibits rosette formation. *Top graph*, LPA_1 knockdown using four distinct shRNAs (qPCR measurements). *Bottom graph*, rosette formation in LPA_1-depleted cells. Quantification was based on >100 fields from two independent experiments. *Error bars*, S.E. A one-sided Student's *t* test was used to indicate significance; *NS*, non-significant; *, $p < 0.05$; **, $p < 0.01$. *D*, pertussis toxin (*PTX*; 200 ng/ml overnight) blocks LPA- and endothelin (*ET*)-induced rosette formation. *Error bars*, S.E. of $n = 12$ (endothelin) and $n = 24$ (LPA) analyzed from live cell imaging videos. A Wilcoxon signed-rank test was used to indicate statistical significance; ***, $p < 0.001$. *a.u.*, arbitrary units.

Src(Y530F) (Fig. 1*D*) had only minor effects on cell morphology (Fig. 1*B*) but led to a marked increase in the number of invadosomes that clustered predominantly at the cell periphery (Fig. 1, *C* and *E*). These actin-rich clusters contained the invadopodial marker Tks5, cortactin, vinculin, and focal adhesion kinase (*FAK*) (Fig. 1*C*). Along with focal adhesion kinase, high levels of phosphotyrosine (*pY*) were also found in these invadosomes (Fig. 1*C*). Of note, invadosome cluster formation was not unique for A375M cells, because very similar structures were also observed in Src(YF)-expressing MDA-MB-435 melanoma cells (see Fig. 2*D*). As expected, invadosome clusters disappeared upon the addition of the Src inhibitor PP2 (results not shown). The Src-induced invadosomes were stable and persisted in serum-free medium, indicating that their formation and maintenance is a cell-intrinsic mechanism, not requiring exogenous growth factors, at least in the presence of active c-Src. The invadosomes were functional in that they colocalized with sites of robust gelatin degradation, a process that was inhibited by the metalloprotease inhibitor GM6001 (Fig. 1, *F* and *G*).

Rapid Formation of ECM-degrading Rosettes by LPA and Endothelin through G_i—We tested a number of GPCR agonists for their ability to influence invadosome abundance and organization in A375M(Src^+) by monitoring actin remodeling using time lapse confocal microscopy. Strikingly, LPA and endothelin induced the rapid formation of highly dynamic invadosome rosettes (Fig. 2, *A* and *B*, and supplemental Video 1). Agonist-induced rosettes displayed various dynamic behaviors as they went through phases of expansion and contraction (supplemental Video 1), a behavior reminiscent of the formation of dynamic podosome rings in osteoclasts (38). Other agonists for which A375M cells express functional receptors (as determined by Ca^{2+} mobilization), including sphingosine 1-phosphate (S1P) and thrombin, showed little or no rosette-inducing capacity. Receptor tyrosine kinase agonists, such as PDGF and VEGF, left invadosome organization similarly unaltered (Fig. 2*A*). Thus, a subclass of GPCRs mediates the rapid remodeling of invadosome clusters into rosettes.

Rosettes appeared within 1 min after LPA or endothelin addition and typically evolved from already existing invadosome clusters at the cell periphery, containing Tks5, cortactin, vinculin, focal adhesion kinase, and enhanced phosphotyrosine (Fig. 2*B*). The newly formed rosettes degraded the ECM in a highly dynamic manner (Fig. 2*C* and supplemental Video 2). LPA-induced rosette formation from pre-existing invadosome clusters was also observed in MDA-MB-435(Src+) melanoma cells (Fig. 2*D*).

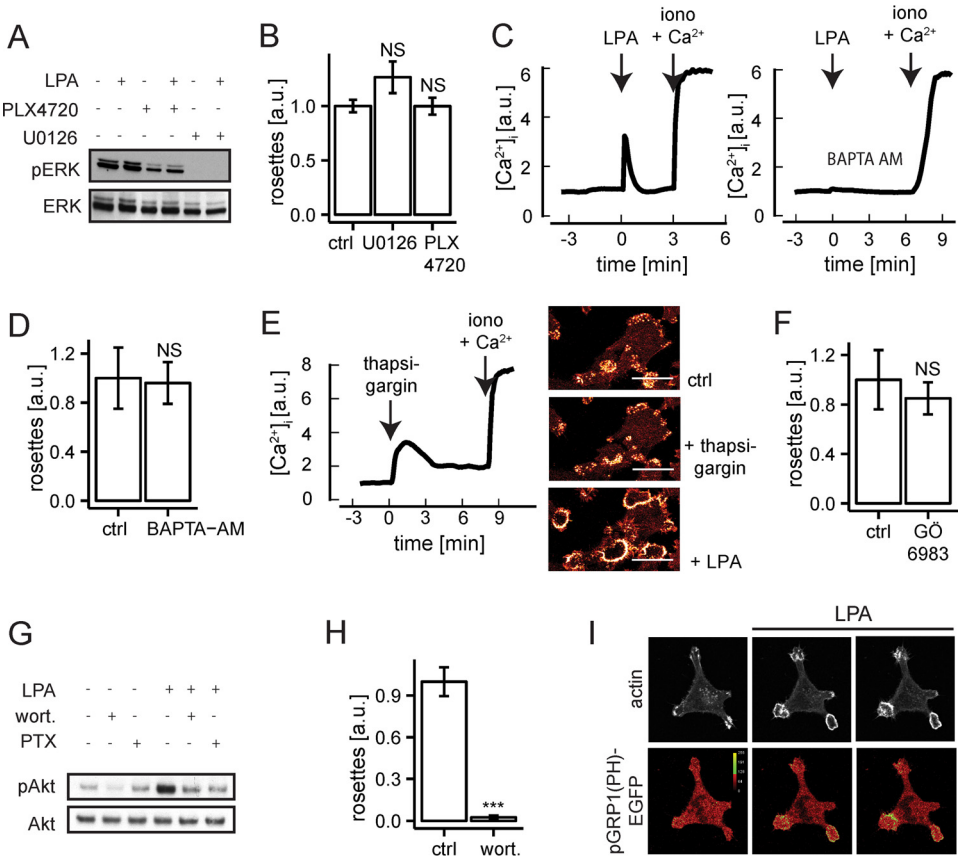

FIGURE 4. **Dissection of signaling pathways in A375M(Src$^+$) cells.** *A*, ERK activation, as measured by phospho-ERK levels. Cells were treated as indicated. B-RAF inhibitor was PLX4720 (1 μM, 2 h); MEK inhibitor was U0126 (10 μM, 1 h). ERK is constitutively active due to oncogenic B-RAF(V600E) expression. *B*, normalized number of rosettes in LPA-stimulated cells exposed to the indicated inhibitors as in *A*. *Error bars*, S.E.; $n = 6$; Student's *t* test; *NS*, non-significant. *C*, LPA-induced Ca^{2+} mobilization (*left*) and its inhibition by BAPTA-AM (*right*). *D*, BAPTA-buffered cells show normal rosette formation by LPA. *Error bars*, S.E. (quantification from 12 live cell videos); Student's *t* test; *NS*, non-significant. *E*, raising cytosolic Ca^{2+} by thapsigargin does not affect rosette formation; nor does PKC inhibition by GÖ6983 (*F*). *Scale bar*, 20 μm. *Error bars* in *F*, S.E.; $n = 4$; Student's *t* test; *NS*, non-significant. *G*, Akt phosphorylation under the indicated conditions: LPA, 5 μM; wortmannin, 100 nM (15 min); PTX (200 ng/ml). *H*, wortmannin blocks LPA-induced rosette formation. *Error bars*, S.E. ($n = 4$); Student's *t* test; ***, $p < 0.001$. *I*, LPA stimulates PIP_3 production specifically at sites of rosette formation. Cells were transfected with LifeAct-RFP along with the PIP_3 biosensor pGRP1(PH)-GFP. Cells were stimulated by LPA for 2 and 4.5 min. *Scale bars*, 10 μm. *a.u.*, arbitrary units.

A375M cells express endothelin B receptors (39), which are known to couple to G_i and G_q (40); furthermore, these cells were found to co-express three distinct LPA receptors, namely LPA_1, LPA_3, and LPA_6 (Fig. 3*A*). The selective LPA_1/LPA_3 antagonist Ki16425 inhibited LPA-induced rosette formation with an IC_{50} value of ~30 nM (Fig. 3*B*), at which dose the inhibitor antagonizes activation of LPA_1 but not LPA_3 (41). Moreover, LPA_1 knockdown cells failed to form rosettes in response to LPA (Fig. 3*C*). We conclude that LPA-induced rosette formation is mediated by the LPA_1 receptor in a non-redundant manner. LPA_1 is known to couple to G_i, $G_{12/13}$, and G_q (25, 42). Pretreatment of the cells with pertussis toxin (PTX) blocked rosette formation by LPA and endothelin (Fig. 3*D*), indicating that invadosome remodeling critically depends on G_i-linked signaling pathways.

Dissection of Signaling Pathways: PI3K, ERK/MAPK, and Ca^{2+}—In addition to Rho family GTPases, G protein-linked effectors and signals implicated in F-actin remodeling include the ERK/MAPK pathway, Ca^{2+} mobilization, and PI3K. Like many melanoma cells, A375M cells express oncogenic B-RAF(V600E), resulting in constitutive activation of the MEK-ERK/MAPK pathway (43). Consistent with this, LPA could not further enhance basal ERK activity (Fig. 4*A*). Inhibitors of B-RAF and MEK (PLX4720 and U0126, respectively) strongly reduced MAPK activity, without affecting pre-existing invadosomes or LPA-induced rosette formation (Fig. 4, *A* and *B*). LPA and endothelin induced a rapid rise in cytosolic Ca^{2+}, which was abrogated by cell-permeable BAPTA-AM (Fig. 4*C*) (results not shown). Ca^{2+}-buffered cells showed fewer invadosome clusters (not shown), but the ability of LPA to induce rosette formation was not affected (Fig. 4*D*). Furthermore, raising cytosolic Ca^{2+} by thapsigargin did not affect rosette formation; nor did the protein kinase C (PKC) inhibitor GÖ6983 (44) (Fig. 3, *E* and *F*). These findings rule out a critical role for ERK/MAPK, Ca^{2+}, and PKC in GPCR-induced invadosome remodeling.

PI3K generates phosphatidyl 3,4,5-trisphosphate (PIP_3) to activate downstream effectors such as Akt. LPA phosphorylated Akt in a PTX- and wortmannin-sensitive manner (Fig. 4*G*). Wortmannin interfered with the maintenance of invadosomes and caused the disassembly of newly formed rosettes (Fig. 4*H*), indicating an indispensable role for basal PI3K activity. Using a PIP_3-specific biosensor, pGRP1(PH)-EGFP (45, 46), we found that LPA stimulates PIP_3 production at the ventral plasma membrane, specifically in the region of rosettes (Fig. 4*I*). We

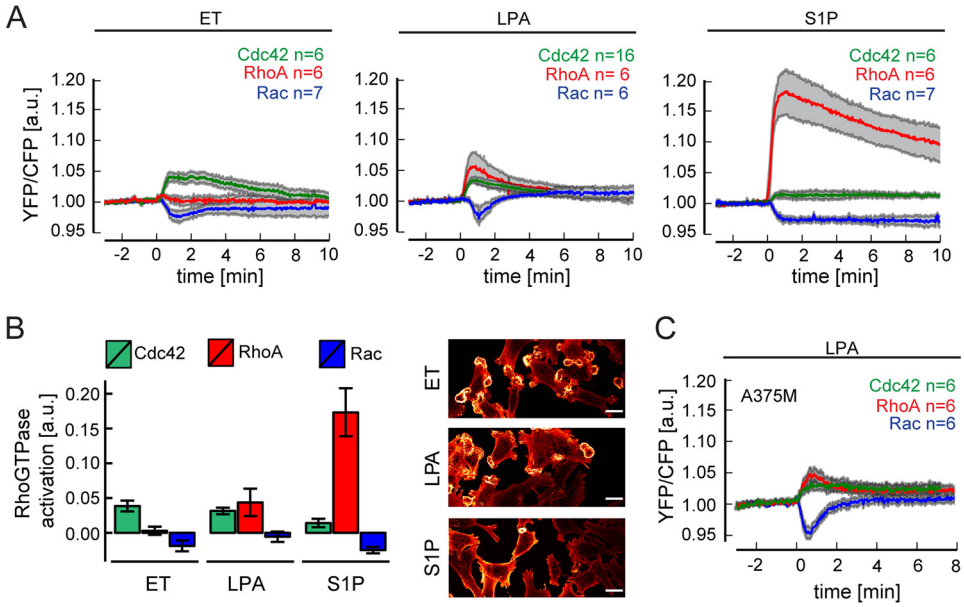

FIGURE 5. **Agonist-induced activities of RhoA, Rac, and Cdc42 monitored in real time.** *A*, activity of the indicated Rho GTPases upon stimulation with endothelin (*ET*), LPA, or S1P, as measured by FRET-based biosensors in A375M(Src$^+$) cells. The YFP/CFP ratio was set to 1.0 at the onset of the experiment. *Traces* show mean responses ± S.E. Mutated inactive biosensors served as negative controls (data not shown). For details, see "Experimental Procedures." *B*, *left*, quantification of Rho GTPases responses. *Bar plots* indicate average signal from 30 to 120 s after the agonist addition. *Error bars*, S.E., as indicated in *A*. *Right*, agonist-induced rosette formation; representative confocal images of F-actin at the ventral plasma membrane at 2 min after the agonist addition. *Scale bar*, 20 μm. Note the correlation with Cdc42 and inverse correlation with RhoA activation. *C*, activity of the indicated Rho GTPases upon LPA stimulation of A375M cells, as measured by FRET-based biosensors. *a.u.*, arbitrary units.

conclude that LPA activates PI3K through G_i, resulting in localized PIP_3 accumulation, serving as an essential signal for rosette formation.

Monitoring Rho GTPase Activities—Rho family GTPases, particularly RhoA, Rac1, and Cdc42, are central regulators of the actin cytoskeleton and implicated in invasive cell migration (47). Cdc42 is known to govern invadosome formation through its downstream effector N-WASP, but much less is known about the role of RhoA and Rac1 in invadosome formation and remodeling (12). We measured the activation of RhoA, Rac1, and Cdc42 by GPCR agonists in real time, using newly developed FRET-based biosensors (see "Experimental Procedures").

As shown in Fig. 5*A*, LPA triggered the rapid co-activation of Cdc42 and RhoA, with very similar kinetics, concurrent with a transient decrease in Rac1 activity. Endothelin, the strongest inducer of invadasome remodeling, similarly enhanced Cdc42 activity with a concomitant reduction in Rac1 activity. Unlike LPA, however, endothelin did not affect RhoA activity (Fig. 5*A*). Peak values of Cdc42 activation and decreased Rac activity were reached at about 1 min (Fig. 5*A*), which coincides with the initiation of rosette formation. We also tested S1P, which showed little or no effect on invadosome remodeling (Fig. 2*A*). When compared with LPA and endothelin, S1P evoked a strikingly robust activation of RhoA and a rather weak Cdc42 activation signal. In addition, S1P rapidly reduced Rac1 activity for a prolonged period of time (>10 min) (Fig. 5*A*). The RhoA response to S1P must be largely mediated by the $S1P_2$ receptor, whose coupling efficiency to the $G_{12/13}$-RhoA pathway is particularly strong (48, 49). Fig. 5*B* summarizes the distinct Rho GTPase responses, showing that Cdc42 activation and Rac deactivation are strongly associated with invadosome remodeling, whereas RhoA activation is inversely correlated and hence may exert an opposing effect. Of note, the pattern of activation and deactivation of RhoGTPases was independent of Src(YF) expression, because A375M cells responded to LPA stimulation in the exact same manner as did A375M(Src$^+$) cells (Fig. 5*C*).

G_i-mediated Activation of Cdc42 Is Essential for Rosette Formation—LPA-induced activation of Cdc42 was almost completely inhibited by PTX (Fig. 6, *A* and *B*), indicating a key role for G_i. Wortmannin inhibited Cdc42 activation by about 40%, indicating that both PI3K-dependent and PI3K-independent pathways downstream of G_i lead to Cdc42 activation. LPA-induced Cdc42 activation was inhibited by Ki16425, confirming LPA_1 involvement (Fig. 6, *A* and *B*). Upon stimulation, Cdc42 was activated predominantly within the rosettes themselves (Fig. 6*C*). Furthermore, rosette formation was impaired upon Cdc42 knockdown using shRNA or by expressing dominant-negative Cdc42(T17N) (Fig. 6, *D* and *E*). Expression of constitutively active Cdc42(Q61L) or Cdc42(F28L) induced the formation of many individual invadosomes, but it prevented LPA from reorganizing them into rosettes (Fig. 6, *E* and *F*). We therefore conclude that a tight spatiotemporal control of Cdc42 activity is critical for agonist-induced rosette formation.

Rac Deactivation Is Non-G_i-mediated—The GPCR-mediated decrease in Rac activity is unexpected, because LPA and other G_i-coupled receptor agonists normally enhance Rac activity as measured by pull-down assays (*e.g.* see Ref. 42). Remarkably, following PTX treatment, the decrease in Rac activity was more pronounced (Fig. 7*A*). It thus appears that the overall Rac signal consists of two components mediated by distinct G proteins: the decrease in Rac activity is non-G_i-mediated and is superimposed by a G_i-mediated increase in Rac activity. Recent evidence indicates that reduced Rac activity promotes invadosome stability, whereas elevated Rac activity drives invadosome dis-

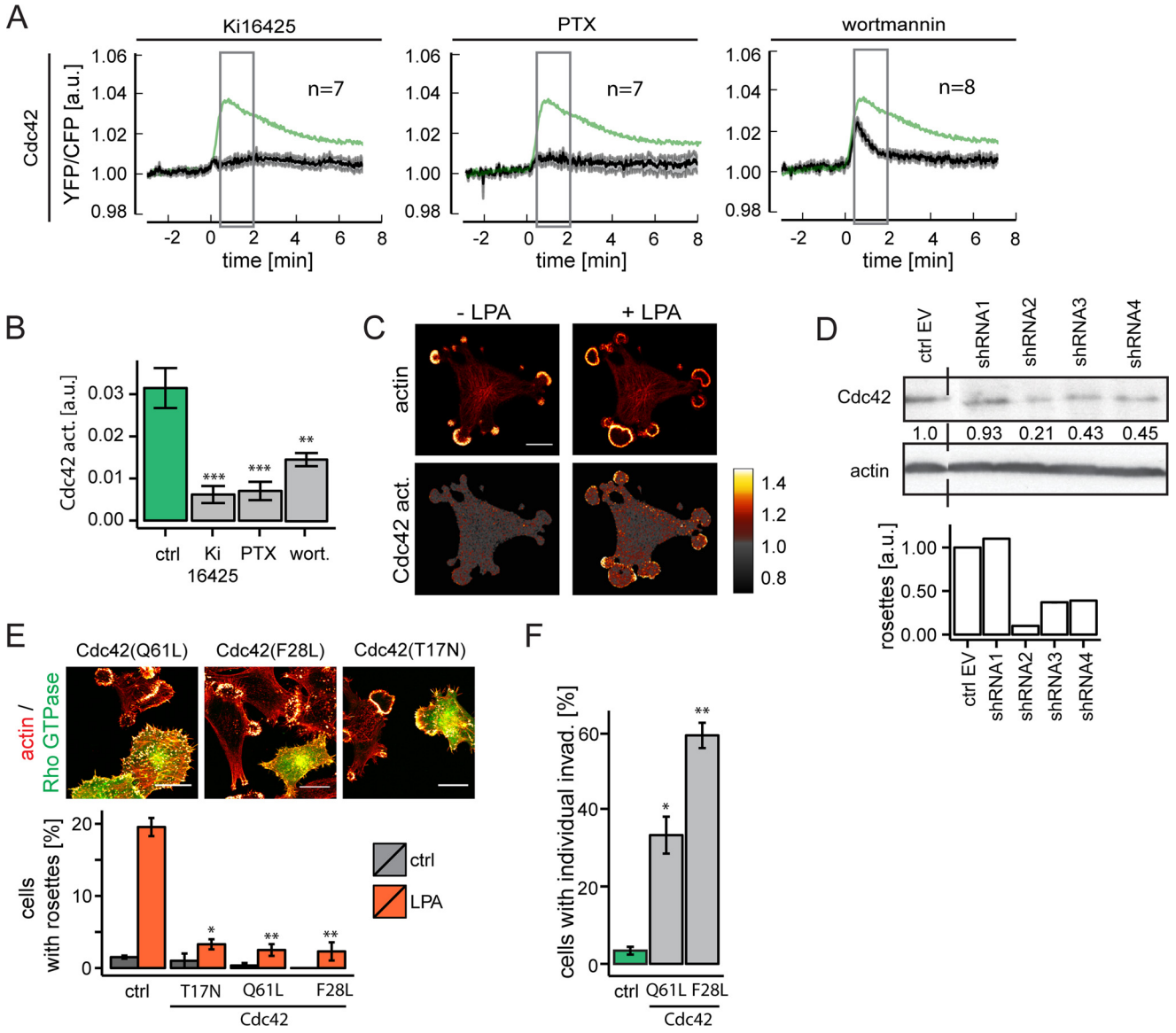

FIGURE 6. **Essential role for transient Cdc42 activation.** *A*, LPA-induced Cdc42 activation and effects of Ki16425, PTX, and wortmannin. The response of untreated cells (control (*ctrl*)) is shown in green ($n = 17$) as in Fig. 5*A*. Data are mean ratio signal ± S.E. *B*, quantification of LPA-induced Cdc42 activation (averaged between 30 and 120 s after stimulation). *Error bars*, S.E.; *n* was as indicated in *A*. Student's *t* test; **, $p < 0.01$; ***, $p < 0.001$. *C*, Cdc42 is activated predominantly in the region of newly formed rosettes. Cdc42 activity is presented as YFP/CFP ratio (set arbitrarily to 1.0 in unstimulated cells). Cells are shown before and at 2.5 min after LPA stimulation; actin was visualized with LifeAct-mCherry. *Scale bar*, 25 μm. *D*, Cdc42 knockdown using four distinct shRNAs prevents LPA-induced rosette formation. *E*, expression of dominant-negative Cdc42(T17N) or constitutively active Cdc42(Q61L) and Cdc42(F28L) mutants interferes with LPA-induced rosette formation. Representative images of cells expressing mutant Cdc42 (marked by GFP) among non-transfected cells. *Scale bars*, 20 μm. The graph (*right*) shows quantification of rosette formation. *Error bars*, S.E.; $n = 3$; Student's *t* test; **, $p < 0.01$; ***, $p < 0.001$. *F*, constitutively active Cdc42 mutants (Q61L and F28L) induce invadosomes but no rosettes (see *E*). *Error bars*, S.E.; $n = 3$; Student's *t* test; *, $p < 0.05$. *a.u.*, arbitrary units.

assembly (14). Consistent with this, expression of constitutively active Rac(QL) abrogated invadosome cluster formation and suppressed rosette formation by LPA (Fig. 7*B*).

RhoA-ROCK Signaling Antagonizes Invadosome Remodeling—The magnitude of agonist-induced RhoA activation showed a marked inverse correlation with rosette formation, suggesting that enhanced RhoA activity suppresses invadosome remodeling. Several lines of experimental evidence support this notion. First, cells expressing active RhoA(V14) lacked invadosome clusters and rosettes (Fig. 7*C*). Second, the ROCK inhibitor Y27632 boosted rosette formation by LPA and endothelin, whereas it conferred rosette-inducing capacity to S1P (Fig. 7*D*). Finally, prior stimulation of the cells with RhoA-activating S1P attenuated the ability of LPA and endothelin to induce rosettes (Fig. 7*E*). From these results, we conclude that the $G_{12/13}$-linked RhoA-ROCK pathway counteracts G_i-Cdc42-mediated rosette formation.

Discussion

Unraveling the signaling inputs and pathways that drive the formation, maintenance, and remodeling of invadopodia is essential to better understand tumor cell invasion into the ECM and surrounding tissues, which is a first step in the metastatic cascade. Numerous molecular components of invadosomes have been identified, and increasing evidence points to their importance *in vivo* (7–10). However, relatively little is still

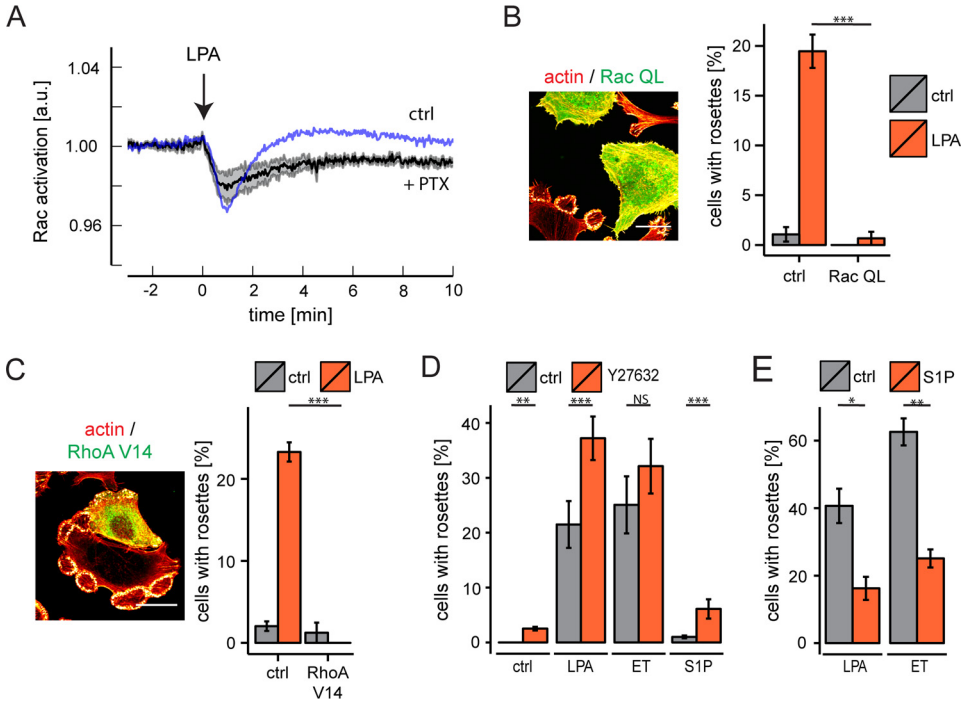

FIGURE 7. **Rac activity and opposing action of RhoA-ROCK signaling.** *A*, effect of PTX on Rac activation in response to LPA. Response of PTX-treated cells ($n = 6$, *black trace*, mean ± S.E.) *versus* non-treated cells (*blue trace*; $n = 8$, as in Fig. 5*A*). PTX treatment reveals biphasic nature of the Rac response. *B*, constitutively active Rac (*Rac QL*) inhibits invadosome cluster formation and largely prevents rosette formation. Shown are representative images of cells expressing constitutively active Rac among non-transfected cells. *Scale bar*, 20 μm. The *bar diagram* shows quantification. *Error bars*, S.E. ($n = 3$); Student's *t* test. *C*, constitutively active RhoA(V14) blocks LPA-induced rosette formation. Representative images (*left*) of cells expressing RhoA(V14) among non-transfected cells. *Scale bars*, 20 μm. The graph (*right*) shows quantification of rosette formation upon LPA stimulation. *Error bars*, S.E.; $n = 3$; Student's *t* test; *NS*, non-significant; ***, $p < 0.001$. *D*, ROCK inhibitor Y27632 boosts rosette formation by LPA, endothelin (*ET*), and S1P. Shown is quantification of ~100 fields from six separate coverslips. *Error bars*, S.E.; two-tailed *p* values were determined by Wilcoxon signed-rank test; **, $p < 0.01$; ***, $p < 0.001$. *E*, pretreatment of the cells with RhoA-activating S1P (2.5 min) attenuates subsequent rosette formation by LPA and endothelin. *Error bars*, S.E.; $n = 3$; Student's *t* test; *, $p < 0.05$; **, $p < 0.01$. *a.u.*, arbitrary units.

known about how pre-existing invadopodia are reassembled into giant rosettes by extracellular cues. Rosette formation is usually assumed to be a spontaneous self-assembly process, but our results indicate that this is not necessarily true.

Our results reveal a previously unknown role for G_i-coupled receptors in driving rosette formation. The use of newly developed FRET-based biosensors allowed us to monitor the kinetics of Rho GTPase responses during agonist-induced rosette formation with high temporal resolution. In our melanoma cell system, active Src promotes invadosome formation and clustering but did not induce rosette formation by itself. Melanoma-relevant GPCR agonists, notably LPA (acting through the LPA_1 receptor) and endothelin (acting via the endothelin B receptor), signal through a G_i-Cdc42 axis to remodel stable Src-induced invadosomes in a highly dynamic manner (Fig. 8). Our results exclude a role for Ca^{2+} mobilization and MAPK activity in the formation of rosettes. Active Cdc42(QL) produced individual invadosomes but failed to form organized rosettes, which emphasizes the importance of a tight spatiotemporal control of Cdc42 activity upon receptor stimulation. The newly formed rosettes rapidly redistribute the ECM-degrading activity, which may help tumor cells to invade the ECM and surrounding tissues in a more efficient and dynamic spatio-temporal manner than stable invadosomes can do. A recent study has implicated EGF as an inducer of rosettes in carcinoma cells (50), although those rosettes lacked ECM-degrading activity.

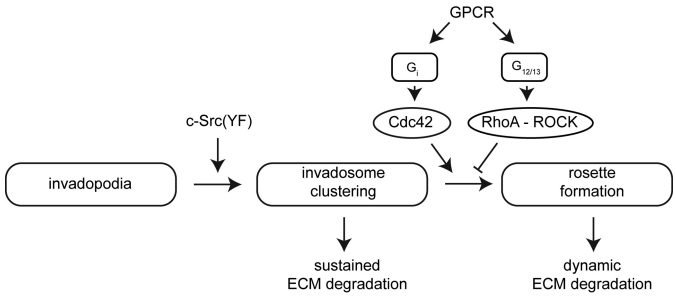

FIGURE 8. **Scheme of invadosome remodeling by G_i-coupled receptors in melanoma cells.** Active c-Src induces stable invadosome clusters in A375M and MDA-MB-435 melanoma cells that are rapidly remodeled into rosettes by G_i-coupled receptor agonists. See "Results" for Rho GTPase signaling details.

LPA stimulated PI3K-mediated PIP_3 production at the ventral membrane, specifically in the region of rosettes. Localized PIP_3 accumulation may serve as an essential signal for rosette formation by recruiting PH domain-containing proteins, including GDP/GTP exchange factors (GEFs) for Rho family GTPases. PI3K exists in distinct isoforms. GPCR agonists activate mainly the β-isoform, so it seems likely that PI3K-β is the main player in our cell system (51, 52). We find that G_i-mediated Cdc42 activation is regulated by both PI3K-dependent and PI3K-independent pathways. This is consistent with the fact that Cd42 activation occurs through multiple pathways, involving both PI3K/PIP_3-driven recruitment of specific GEFs and direct interaction of G(βγ) subunits with specific GEFs (52–

54). Given the multitude of Cdc42/Rac-specific GEFs in most cell types, it is too early to speculate about the identity of the GEF(s) involved.

G_i-mediated activation of Cdc42 was accompanied by a rapid fall in Rac activity. This unexpected Rac response could be dissected into two components: a G_i-mediated increase in Rac activity and a non-G_i-mediated decrease in Rac-GTP. The latter phase was dominant over the first. RhoA and Rac are known to oppose each other at multiple levels, and their activity balance orchestrates cell shape, migration, and invasion (55–57). Active RhoA can inhibit Rac through activation of a GTPase-activating protein (58). However, the decrease in Rac activity observed here cannot be attributed to RhoA activation, because endothelin lowered Rac activity without activating RhoA. Therefore, it is more likely that Rac is inhibited through G_q-mediated phospholipase C activation, a scenario that needs to be further explored. Whatever the mechanism of Rac deactivation, our results are consistent with recent evidence suggesting that decreased Rac1 activity is necessary for maintaining invadosome stability (14). The finding that active Rac(QL) prevents rosette formation lends further support to this view. We therefore propose that deactivated Rac cooperates with active Cdc42 to promote rosette assembly. Finally, we show that the well established $G_{12/13}$-RhoA-ROCK signaling pathway antagonizes invadosome remodeling. Thus, GPCR agonists that do not activate the $G_{12/13}$-linked RhoA activation are predicted to be the most efficient inducers of rosette formation, as we indeed found here for endothelin.

In conclusion, our study reveals G_i-coupled receptor agonists, notably LPA and endothelin, as potent inducers of rosette formation in the context of active c-Src. The degree of invadosome remodeling is dictated by the Cdc42-RhoA activity balance, with a likely modulatory role for Rac deactivation. Determination of precisely how the activities of the distinct Rho GTPases are regulated and coordinated during agonist-induced invadosome remodeling remains a challenge for further studies.

Author Contributions—K. J. and W. H. M. conceived and coordinated the study and wrote the paper together with K. M. K. K. M. K. designed, performed, and analyzed most of the experiments. D. L.-P. and E. A. performed biochemical experiments. A. J. B. and B. v. B. performed biophysical experiments. T. Y. and Y. I. W. designed FRET-based biosensors. F. N. v. L. designed and supervised the matrix degradation assays. M. I. designed and supervised the Rho GTPase assays.

Acknowledgments—We thank members of the Division of Cell Biology for stimulating discussions, Dr. Bram van den Broek for video processing, and Jeffrey Klarenbeek for constructs.

References

1. Linder, S., Wiesner, C., and Himmel, M. (2011) Degrading devices: invadosomes in proteolytic cell invasion. *Annu. Rev. Cell Dev. Biol.* **27,** 185–211
2. Murphy, D. A., and Courtneidge, S. A. (2011) The "ins" and "outs" of podosomes and invadopodia: characteristics, formation and function. *Nat. Rev. Mol. Cell Biol.* **12,** 413–426
3. Bravo-Cordero, J. J., Hodgson, L., and Condeelis, J. (2012) Directed cell invasion and migration during metastasis. *Curr. Opin. Cell Biol.* **24,** 277–283
4. Beaty, B. T., and Condeelis, J. (2014) Digging a little deeper: the stages of invadopodium formation and maturation. *Eur. J. Cell Biol.* **93,** 438–444
5. Buccione, R., Orth, J. D., and McNiven, M. A. (2004) Foot and mouth: podosomes, invadopodia and circular dorsal ruffles. *Nat. Rev. Mol. Cell Biol.* **5,** 647–657
6. Hoshino, D., Branch, K. M., and Weaver, A. M. (2013) Signaling inputs to invadopodia and podosomes. *J. Cell Sci.* **126,** 2979–2989
7. Hagedorn, E. J., Ziel, J. W., Morrissey, M. A., Linden, L. M., Wang, Z., Chi, Q., Johnson, S. A., and Sherwood, D. R. (2013) The netrin receptor DCC focuses invadopodia-driven basement membrane transmigration *in vivo*. *J. Cell Biol.* **201,** 903–913
8. Leong, H. S., Robertson, A. E., Stoletov, K., Leith, S. J., Chin, C. A., Chien, A. E., Hague, M. N., Ablack, A., Carmine-Simmen, K., McPherson, V. A., Postenka, C. O., Turley, E. A., Courtneidge, S. A., Chambers, A. F., and Lewis, J. D. (2014) Invadopodia are required for cancer cell extravasation and are a therapeutic target for metastasis. *Cell Rep.* **8,** 1558–1570
9. Seano, G., Chiaverina, G., Gagliardi, P. A., di Blasio, L., Puliafito, A., Bouvard, C., Sessa, R., Tarone, G., Sorokin, L., Helley, D., Jain, R. K., Serini, G., Bussolino, F., and Primo, L. (2014) Endothelial podosome rosettes regulate vascular branching in tumour angiogenesis. *Nat. Cell Biol.* **16,** 931- 941
10. Génot, E., and Gligorijevic, B. (2014) Invadosomes in their natural habitat. *Eur. J. Cell Biol.* **93,** 367–379
11. Boateng, L. R., and Huttenlocher, A. (2012) Spatiotemporal regulation of Src and its substrates at invadosomes. *Eur. Cell Biol.* **91,** 878–888
12. Spuul, P., Ciufici, P., Veillat, V., Leclercq, A., Daubon, T., Kramer, I. J., and Genot, E. (2014) Importance of RhoGTPases in formation, characteristics, and functions of invadosomes. *Small GTPases* **5,** e28195
13. Nakahara, H., Otani, T., Sasaki, T., Miura, Y., Takai, Y., and Kogo, M. (2003) Involvement of Cdc42 and Rac small G proteins in invadopodia formation of RPMI7951 cells. *Genes Cells* **8,** 1019–1027
14. Moshfegh, Y., Bravo-Cordero, J. J., Miskolci, V., Condeelis, J., and Hodgson, L. (2014) A Trio-Rac1-Pak1 signalling axis drives invadopodia disassembly. *Nat. Cell Biol.* **16,** 574–586
15. Sun, J., Lu, F., He, H., Shen, J., Messina, J., Mathew, R., Wang, D., Sarnaik, A. A., Chang, W. C., Kim, M., Cheng, H., and Yang, S. (2014) STIM1- and Orai1-mediated Ca^{2+} oscillation orchestrates invadopodium formation and melanoma invasion. *J. Cell Biol.* **207,** 535–548
16. Eckert, M. A., Lwin, T. M., Chang, A. T., Kim, J., Danis, E., Ohno-Machado, L., and Yang, J. (2011) Twist1-induced invadopodia formation promotes tumor metastasis. *Cancer Cell* **19,** 372–386
17. Pignatelli, J., Tumbarello, D. A., Schmidt, R. P., and Turner, C. E. (2012) Hic-5 promotes invadopodia formation and invasion during TGF-β-induced epithelial-mesenchymal transition. *J. Cell Biol.* **197,** 421–437
18. Rajadurai, C. V., Havrylov, S., Zaoui, K., Vaillancourt, R., Stuible, M., Naujokas, M., Zuo, D., Tremblay, M. L., and Park, M. (2012) Met receptor tyrosine kinase signals through a cortactin-Gab1 scaffold complex, to mediate invadopodia. *J. Cell Sci.* **125,** 2940–2953
19. Kocher, H. M., Sandle, J., Mirza, T. A., Li, N. F., and Hart, I. R. (2009) Ezrin interacts with cortactin to form podosomal rosettes in pancreatic cancer cells. *Gut* **58,** 271–284
20. Pan, Y. R., Chen, C. L., and Chen, H. C. (2011) FAK is required for the assembly of podosome rosettes. *J. Cell Biol.* **195,** 113–129
21. David-Pfeuty, T., and Singer, S. J. (1980) Altered distributions of the cytoskeletal proteins vinculin and α-actinin in cultured fibroblasts transformed by Rous sarcoma virus. *Proc. Natl. Acad. Sci. U.S.A.* **77,** 6687–6691
22. Akisaka, T., Yoshida, H., Inoue, S., and Shimizu, K. (2001) Organization of cytoskeletal F-actin, G-actin, and gelsolin in the adhesion structures in cultured osteoclast. *J. Bone Miner. Res.* **16,** 1248–1255
23. Varon, C., Tatin, F., Moreau, V., Van Obberghen-Schilling, E., Fernandez-Sauze, S., Reuzeau, E., Kramer, I., and Génot, E. (2006) Transforming growth factor β induces rosettes of podosomes in primary aortic endothelial cells. *Mol. Cell. Biol.* **26,** 3582–3594
24. Moolenaar, W. H. (1995) Lysophosphatidic acid, a multifunctional phospholipid messenger. *J. Biol. Chem.* **270,** 12949–12952
25. Choi, J. W., Herr, D. R., Noguchi, K., Yung, Y. C., Lee, C. W., Mutoh, T., Lin, M. E., Teo, S. T., Park, K. E., Mosley, A. N., and Chun, J. (2010) LPA

receptors: subtypes and biological actions. *Annu. Rev. Pharmacol. Toxicol.* **50,** 157–186
26. Umezu-Goto, M., Kishi, Y., Taira, A., Hama, K., Dohmae, N., Takio, K., Yamori, T., Mills, G. B., Inoue, K., Aoki, J., and Arai, H. (2002) Autotaxin has lysophospholipase D activity leading to tumor cell growth and motility by lysophosphatidic acid production. *J. Cell Biol.* **158,** 227–233
27. van Meeteren, L. A., and Moolenaar, W. H. (2007) Regulation and biological activities of the autotaxin-LPA axis. *Prog. Lipid Res.* **46,** 145–160
28. Liu, S., Umezu-Goto, M., Murph, M., Lu, Y., Liu, W., Zhang, F., Yu, S., Stephens, L. C., Cui, X., Murrow, G., Coombes, K., Muller, W., Hung, M. C., Perou, C. M., Lee, A. V., Fang, X., and Mills, G. B. (2009) Expression of autotaxin and lysophosphatidic acid receptors increases mammary tumorigenesis, invasion, and metastases. *Cancer Cell* **15,** 539–550
29. Marshall, J. C., Collins, J. W., Nakayama, J., Horak, C. E., Liewehr, D. J., Steinberg, S. M., Albaugh, M., Vidal-Vanaclocha, F., Palmieri, D., Barbier, M., Murone, M., and Steeg, P. S. (2012) Effect of inhibition of the lysophosphatidic acid receptor 1 on metastasis and metastatic dormancy in breast cancer. *J. Natl. Cancer Inst.* **104,** 1306–1319
30. Houben, A. J., and Moolenaar, W. H. (2011) Autotaxin and LPA receptor signaling in cancer. *Cancer Metastasis Rev.* **30,** 557–565
31. Saldana-Caboverde, A., and Kos, L. (2010) Roles of endothelin signaling in melanocyte development and melanoma. *Pigment Cell Melanoma Res.* **23,** 160–170
32. Bagnato, A., and Rosanò, L. (2008) The endothelin axis in cancer. *Int. J. Biochem. Cell Biol.* **40,** 1443–1451
33. Asundi, J., Reed, C., Arca, J., McCutcheon, K., Ferrando, R., Clark, S., Luis, E., Tien, J., Firestein, R., and Polakis, P. (2011) An antibody-drug conjugate targeting the endothelin B receptor for the treatment of melanoma. *Clin. Cancer Res.* **17,** 965–975
34. Itoh, R. E., Kurokawa, K., Ohba, Y., Yoshizaki, H., Mochizuki, N., and Matsuda, M. (2002) Activation of rac and cdc42 video imaged by fluorescent resonance energy transfer-based single-molecule probes in the membrane of living cells. *Mol. Cell. Biol.* **22,** 6582–6591
35. Yoshizaki, H., Ohba, Y., Kurokawa, K., Itoh, R. E., Nakamura, T., Mochizuki, N., Nagashima, K., and Matsuda, M. (2003) Activity of Rho-family GTPases during cell division as visualized with FRET-based probes. *J. Cell Biol.* **162,** 223–232
36. Pertz, O., Hodgson, L., Klemke, R. L., and Hahn, K. M. (2006) Spatiotemporal dynamics of RhoA activity in migrating cells. *Nature* **440,** 1069–1072
37. Schindelin, J., Arganda-Carreras, I., Frise, E., Kaynig, V., Longair, M., Pietzsch, T., Preibisch, S., Rueden, C., Saalfeld, S., Schmid, B., Tinevez, J. Y., White, D. J., Hartenstein, V., Eliceiri, K., Tomancak, P., and Cardona, A. (2012) Fiji: an open-source platform for biological-image analysis. *Nat. Methods* **9,** 676–682
38. Destaing, O., Saltel, F., Géminard, J. C., Jurdic, P., and Bard, F. (2003) Podosomes display actin turnover and dynamic self-organization in osteoclasts expressing actin-green fluorescent protein. *Mol. Biol. Cell* **14,** 407–416
39. Okazawa, M., Shiraki, T., Ninomiya, H., Kobayashi, S., and Masaki, T. (1998) Endothelin-induced apoptosis of A375 human melanoma cells. *J. Biol. Chem.* **273,** 12584–12592
40. Sandoval, Y. H., Atef, M. E., Levesque, L. O., Li, Y., and Anand-Srivastava, M. B. (2014) Endothelin-1 signaling in vascular physiology and pathophysiology. *Curr. Vasc. Pharmacol.* **12,** 202–214
41. Ohta, H., Sato, K., Murata, N., Damirin, A., Malchinkhuu, E., Kon, J., Kimura, T., Tobo, M., Yamazaki, Y., Watanabe, T., Yagi, M., Sato, M., Suzuki, R., Murooka, H., Sakai, T., Nishitoba, T., Im, D. S., Nochi, H., Tamoto, K., Tomura, H., and Okajima, F. (2003) Ki16425, a subtype-selective antagonist for EDG-family lysophosphatidic acid receptors. *Mol. Pharmacol.* **64,** 994–1005
42. Van Leeuwen, F. N., Olivo, C., Grivell, S., Giepmans, B. N., Collard, J. G., and Moolenaar, W. H. (2003) Rac activation by lysophosphatidic acid LPA1 receptors through the guanine nucleotide exchange factor Tiam1. *J. Biol. Chem.* **278,** 400–406
43. Packer, L. M., East, P., Reis-Filho, J. S., and Marais, R. (2009) Identification of direct transcriptional targets of (V600E)BRAF/MEK signalling in melanoma. *Pigment Cell Melanoma Res.* **22,** 785–798
44. Gschwendt, M., Dieterich, S., Rennecke, J., Kittstein, W., Mueller, H. J., and Johannes, F. J. (1996) Inhibition of protein kinase C μ by various inhibitors: differentiation from protein kinase C isoenzymes. *FEBS Lett.* **392,** 77–80
45. Gray, A., Van Der Kaay, J., and Downes, C. P. (1999) The pleckstrin homology domains of protein kinase B and GRP1 (general receptor for phosphoinositides-1) are sensitive and selective probes for the cellular detection of phosphatidylinositol 3,4-bisphosphate and/or phosphatidylinositol 3,4,5-trisphosphate *in vivo*. *Biochem. J.* **344,** 929–936
46. Jongsma, M., Matas-Rico, E., Rzadkowski, A., Jalink, K., and Moolenaar, W. H. (2011) LPA is a chemorepellent for B16 melanoma cells: action through the cAMP-elevating LPA5 receptor. *PLoS One* **6,** e29260
47. Ridley, A. J. (2015) Rho GTPase signalling in cell migration. *Curr. Opin. Cell Biol.* **36,** 103–112
48. Lepley, D., Paik, J. H., Hla, T., and Ferrer, F. (2005) The G protein-coupled receptor S1P2 regulates Rho/Rho kinase pathway to inhibit tumor cell migration. *Cancer Res.* **65,** 3788–3795
49. Skoura, A., and Hla, T. (2009) Regulation of vascular physiology and pathology by the S1P2 receptor subtype. *Cardiovasc. Res.* **82,** 221–228
50. Marchesin, V., Montagnac, G., and Chavrier, P. (2015) ARF6 promotes the formation of Rac1 and WAVE-dependent ventral F-actin rosettes in breast cancer cells in response to epidermal growth factor. *PLoS One* **10,** e0121747
51. Vanhaesebroeck, B., Guillermet-Guibert, J., Graupera, M., and Bilanges, B. (2010) The emerging mechanisms of isoform-specific PI3K signalling. *Nat. Rev. Mol. Cell Biol.* **11,** 329–341
52. Fritsch, R., de Krijger, I., Fritsch, K., George, R., Reason, B., Kumar, M. S., Diefenbacher, M., Stamp, G., and Downward, J. (2013) RAS and RHO families of GTPases directly regulate distinct phosphoinositide 3-kinase isoforms. *Cell* **153,** 1050–1063
53. Sinha, S., and Yang, W. (2008) Cellular signaling for activation of Rho GTPase Cdc42. *Cell. Signal.* **20,** 1927–1934
54. Ueda, H., Nagae, R., Kozawa, M., Morishita, R., Kimura, S., Nagase, T., Ohara, O., Yoshida, S., and Asano, T. (2008) Heterotrimeric G protein $\beta\gamma$ subunits stimulate FLJ00018, a guanine nucleotide exchange factor for Rac1 and Cdc42. *J. Biol. Chem.* **283,** 1946–1953
55. Guilluy, C., Garcia-Mata, R., and Burridge, K. (2011) Rho protein crosstalk: another social network? *Trends Cell Biol.* **21,** 718–726
56. Leeuwen, F. N., Kain, H. E., Kammen, R. A., Michiels, F., Kranenburg, O. W., and Collard, J. G. (1997) The guanine nucleotide exchange factor Tiam1 affects neuronal morphology: opposing roles for the small GTPases Rac and Rho. *J. Cell Biol.* **139,** 797–807
57. Sander, E. E., ten Klooster, J. P., van Delft, S., van der Kammen, R. A., and Collard, J. G. (1999) Rac downregulates Rho activity: reciprocal balance between both GTPases determines cellular morphology and migratory behavior. *J. Cell Biol.* **147,** 1009–1022
58. Nakamura, F. (2013) FilGAP and its close relatives: a mediator of Rho-Rac antagonism that regulates cell morphology and migration. *Biochem. J.* **453,** 17–25
59. Artym, V. V., Yamada, K. M., and Mueller, S. C. (2009) ECM degradation assays for analyzing local cell invasion. *Methods Mol. Biol.* **522,** 211–219
60. Langeslag, M., Clark, K., Moolenaar, W. H., van Leeuwen, F. N., and Jalink, K. (2007) Activation of TRPM7 channels by phospholipase C-coupled receptor agonists. *J. Biol. Chem.* **282,** 232–239

Rapid Remodeling of Invadosomes by G_i-coupled Receptors: DISSECTING THE ROLE OF Rho GTPases

Katarzyna M. Kedziora, Daniela Leyton-Puig, Elisabetta Argenzio, Anja J. Boumeester, Bram van Butselaar, Taofei Yin, Yi I. Wu, Frank N. van Leeuwen, Metello Innocenti, Kees Jalink and Wouter H. Moolenaar

J. Biol. Chem. 2016, 291:4323-4333.
doi: 10.1074/jbc.M115.695940 originally published online January 6, 2016